Spatial Inequalities in U.S. Electric Vehicle Infrastructure

Sechindra Vallury[a], Ravneet Kaur[b]

[a] *Odum School of Ecology, 203 D.W. Brooks Dr., Athens, 30602, GA, USA*
[b] *Warnell School of Forestry & Natural Resources, 180 E Green St, Athens, 30602, GA, USA*

Abstract

Equitable decarbonization depends not only on technology adoption but also on how infrastructure is deployed. Because infrastructure is fixed in space and path dependent, new investments can lock in advantage or exclusion for decades. We examine this dynamic in the case of federal electric vehicle infrastructure, where equity shortfalls are not merely local disparities but structural outcomes of spatial interdependence. Using geospatial analysis and spatial econometric models across 15,566 census tracts in ten southeastern U.S. states, we find that disadvantaged communities are on average 53% farther from federally designated Alternative Fuel Corridors, and that spillovers from neighboring burdens add an additional 10% disadvantage. To test whether inequities are inevitable or policy-contingent, we simulate a counterfactual reallocation aligned with Justice40 mandates. This scenario reduces the average distance gap by 40% and spillover disadvantage by more than 60%. Equity shortfalls in infrastructure transitions thus arise structurally from legacy siting and spatial spillovers, but they are not immutable. Targeted interventions can realign outcomes, showing how network-aware equity frameworks can make the clean energy transition both more just and more effective.

Keywords: electric vehicle infrastructure, spatial equity, Justice40, spatial econometrics, energy policy

1. Introduction

Infrastructure has long reflected and reinforced racial and social inequalities. Because it is fixed in space and durable over time, new investments often

reproduce historical patterns of exclusion [1, 2]. The U.S. highway system, for example, disproportionately displaced Black and low-income communities and entrenched long-term disparities in mobility, environmental exposure, and neighborhood investment [3, 4, 5]. Similar inequities are evident across broadband, stormwater, and other systems, where access has closely followed the contours of race, income, and political influence [6, 7, 8]. In this context, public investment in clean energy infrastructure presents both an opportunity and a risk: without deliberate attention to design and siting, the energy transition may reproduce existing geographies of inequality.

Infrastructure inequalities matter for at least four reasons. First, they determine who can participate in low-carbon transitions: absent infrastructure, households and communities are effectively excluded from clean mobility, energy, and opportunity [9]. Second, because infrastructure is path dependent, present-day allocation decisions can entrench inequities for decades, locking in exclusion and foreclosing future options [10]. Third, inequalities are compounded through spatial spillovers: the burdens of one community can shape those of its neighbors. If infrastructure investments bypass a disadvantaged area, surrounding communities may also face reduced access, slower modernization, and diminished ecosystem services and prospects for investment, creating regional clusters of exclusion rather than isolated gaps [2, 11]. Fourth, while climate policy mandates are rapidly expanding infrastructure investments, planning frameworks often lack spatially explicit equity criteria, raising the risk that programs reinforce rather than redress entrenched disparities [12].

These dynamics are especially salient in the transition to electric vehicles (EVs), where charging infrastructure determines who can participate in the clean energy transition. A growing body of research examines equity in EV charging networks, typically by comparing charger density or proximity across neighborhoods [13, 14, 15, 16]. These studies consistently show that demand-driven and private-sector siting favors affluent, high-density areas, leaving historically disadvantaged communities under-served. Yet this literature largely treats communities in isolation, overlooking how access is shaped by legacy networks and the characteristics of surrounding areas. Our study addresses this gap by analyzing how spatial spillovers and infrastructural legacies condition equity outcomes in federally funded infrastructure programs.

Our empirical setting is the U.S. National Electric Vehicle Infrastructure (NEVI) Formula Program, a $5 billion federal initiative created under the

2021 Infrastructure Investment and Jobs Act [17, 18]. NEVI is the first federally funded EV charging program with an explicit equity mandate, requiring that 40% of benefits accrue to disadvantaged communities (DACs) under the Justice40 Initiative. Its implementation occurs in two stages: first, the buildout of Alternative Fuel Corridors (AFCs) along highways, followed by community and non-corridor investments once corridor requirements are met. This design makes NEVI an ideal case for studying whether legacy infrastructure networks, such as the U.S. highway system that is itself an artifact of racial and spatial inequality, constrain the pursuit of equitable energy transitions [3, 4, 5].

We argue that spatial spillovers are a critical, under-examined mechanism through which justice-focused infrastructure programs can fall short. Even when a disadvantaged community receives direct investment, its access is conditioned by the geography of neighboring areas and by the legacy systems on which new infrastructure is built. To investigate this, we use a geospatial dataset linking census tract-level burdens from the Climate and Economic Justice Screening Tool (CEJST) with AFCs proposed under the NEVI program across ten southeastern U.S. states. Using spatial econometric models, we examine whether disadvantaged communities are systematically located farther from federally funded EV infrastructure and how spatial interdependencies shape access outcomes.

Our results reveal two dynamics. First, disadvantaged communities are systematically farther from AFCs. Second, spatial spillovers amplify inequities, such that even when a tract has relatively low burdens, being surrounded by disadvantaged neighbors can reduce its access to AFCs. To investigate whether such inequities are inevitable, we simulate a counterfactual equity scenario that reallocates proposed AFCs siting to approximate Justice40's mandate. This exercise demonstrates that equity shortfalls in infrastructure transitions arise structurally from legacies and spatial spillovers, but that modest policy interventions can substantially reduce them. By foregrounding spillovers and legacy effects, our analysis contributes a broader framework for understanding equity in infrastructure transitions. While our empirical case is EV infrastructure, the implications extend to other justice-focused investments, such as broadband, flood resilience, and water systems, where spatial interdependencies and legacy infrastructures shape distributive outcomes, and where equity programs may fall short if they fail to address these structural dynamics.

2. Methods

2.1. Study Area and Data Sources

Our analysis examines spatial disparities in access to electric vehicle (EV) charging infrastructure under the National Electric Vehicle Infrastructure (NEVI) Formula Program across ten southeastern U.S. states. These states: Alabama, Arkansas, Florida, Georgia, Kentucky, Louisiana, Mississippi, North Carolina, South Carolina, and Tennessee were selected based on the U.S. Fish and Wildlife Service's southeastern regional classification. The AFC shapefile was retrieved from the U.S. Department of Transportation's ArcGIS Hub in May 2024 [19]. Puerto Rico and the Virgin Islands were initially considered but excluded from the final sample due to missing or incompatible AFC shapefiles [19] and the absence of an interstate highway network [20], respectively.

Census tract geometries were obtained from the U.S. Census TIGER/Line shapefiles and projected into NAD83 / Conus Albers for spatial consistency. DAC designations and associated percentile scores were retrieved from the White House Council on Environmental Quality's Climate and Economic Justice Screening Tool (CEJST v1.0), accessed in May 2024 via the CEJST geoplatform [21]. CEJST provides a binary classification of DACs alongside a comprehensive set of percentile-based indicators covering environmental, climate, and socioeconomic burdens. These percentiles reflect the relative standing of each tract nationally across multiple dimensions such as energy burden, fine particulate matter ($PM_{2.5}$) exposure, diesel emissions, and poverty. The binary DAC flag also includes tracts that, while not meeting every threshold, are low-income and surrounded entirely by DAC-designated neighbors—an imputation that supports spatial contiguity in justice designations. Unlike the Department of Energy's DCR tool, which uses state-specific percentile cutoffs and emphasizes energy-specific burdens, CEJST's national percentile structure enables more consistent cross-state analysis. We opted for CEJST due to its broader coverage and compatibility with our national percentile-based modeling approach, noting that CEJST and DOE DAC classifications exhibit substantial overlap. In addition to spatial justice data from CEJST, we used the 2010 Census Geocoder to classify whether a census tract is urban or rural.

Across the study region, the final dataset encompassed 15,566 census tracts. Tract areas varied widely, ranging from under 1 to over 600 square kilometers, with a right-skewed distribution and a median of approximately

123 square kilometers (see Appendix Fig. A1). This spatial heterogeneity—particularly across rural and exurban zones—underscores the importance of using geometric centroids rather than population-weighted centroids for proximity analysis, especially in a context where infrastructure corridors are linear and spatially discontinuous. We calculated proximity using ArcGIS's "Near" tool, measuring the distance from each tract centroid to the nearest AFC segment within a 100-mile (527,999 ft) search radius. This buffer ensured that all tracts, including rural and remote areas, returned valid distance values, consistent with NEVI's 50-mile spacing benchmark. Spatial contiguity was defined using a first-order Queen criterion, producing neighborhood sizes that ranged from 1 to 25 tracts, with a median of 6 (Appendix Fig. A2). This structure preserves both topological and boundary adjacency and provides a stable basis for capturing spatial dependence across varied tract morphologies.

2.2. Proximity to EV Infrastructure

To assess spatial access to NEVI-funded EV infrastructure, we computed straight-line (Euclidean) distances from the geographic centroid of each census tract to the nearest proposed Alternative Fuel Corridor (AFC). Geographic centroids were calculated using ArcGIS Pro's "Feature to Point" tool. We then applied the "Near" tool with a 100-mile (160.9 km) search radius to ensure connectivity in sparsely served states. An initial threshold of 75 miles failed to resolve proximity for many rural tracts. Output distances were calculated in survey feet and subsequently converted to miles.

To isolate access gaps associated specifically with the NEVI siting process rather than legacy infrastructure disparities, we replicated the centroid-to-corridor distance analysis using the full U.S. interstate highway network as a baseline comparator. This benchmarking isolates equity gaps arising from NEVI-specific deployment decisions, separating them from historical disparities embedded in the legacy highway network. To move beyond descriptive proximity patterns and quantify the spatial structure of observed disparities, we used spatial econometric modeling.

2.3. Spatial Durbin Model

We estimated a Spatial Durbin Model (SDM) to assess whether disparities in AFC proximity are spatially structured and subject to spillover effects. The SDM extends standard linear regression by incorporating spatial lags of both the dependent variable and the covariates, allowing us to capture both

direct (within-tract) and indirect (neighboring-tract) effects [22]. The model is formally specified as:

$$y = \rho W y + X\beta + WX\theta + \varepsilon, \tag{1}$$

where y is the vector of logged distances from each tract centroid to the nearest AFC, X is a matrix of tract-level predictors, W is a row-standardized first-order Queen contiguity weights matrix, ρ is the spatial autoregressive coefficient, θ captures the spatial lag of the covariates, and ε is a normally distributed error term.

Our predictor matrix includes the binary DAC classification from CEJST, along with percentiles for diesel particulate matter, fine particulate matter ($PM_{2.5}$), poverty rate, energy burden, housing cost burden, and agricultural land conversion risk (see Appendix Table A.1 for the full list of predictor variables and their corresponding Justice40 burden categories). We also include the log-transformed distance to the nearest interstate highway to capture infrastructural connectedness while correcting for skewness. All variables except the DAC binary and freeway distance are in percentiles, as provided by CEJST. This avoids arbitrary thresholds and maintains comparability across states and dimensions.

We used bootstrapped standard errors based on 1,000 replications to ensure inference robustness. Following estimation, we decomposed total effects into direct effects (representing a covariate's impact on the tract's own outcome), indirect effects (spillover effects from neighboring tracts), and total effects (the sum of direct and indirect impacts). This decomposition makes visible how local and neighboring structural burdens interact to shape spatial disparities in infrastructure access. Appendix A.3 reports the full SDM coefficient estimates and robustness checks. Prior to model estimation, we conducted spatial autocorrelation diagnostics, including Moran's I and Lagrange Multiplier tests, and compared model fit against spatial error and spatial lag alternatives to confirm the presence of spatial dependence and justify the use of a Spatial Durbin Model (see Appendix sections A.1 and A.2).

2.4. Augmented Inverse Probability Weighting Model

To evaluate whether disparities in AFC proximity by DAC status persist after accounting for structural confounding, we implemented an augmented inverse probability weighting (AIPW, or doubly robust) estimator. AIPW

reweights the sample to balance DAC and non-DAC tracts on observed covariates, thereby reducing bias from structural differences such as poverty, pollution, and network proximity. We used stabilized weights and trimmed observations outside the 1st and 99th percentiles to ensure overlap and reduce variance [23, 24, 25].

Let $D_i \in \{0, 1\}$ indicate DAC status under CEJST v1.0, and let $Y_i = \log(\text{distance to nearest AFC}_i)$. With covariates X_i (CEJST percentiles and log freeway distance), we first estimate the propensity score

$$\hat{e}(X_i) = P(D_i = 1 \mid X_i),$$

construct stabilized weights

$$w_i = \frac{D_i \cdot P(D = 1)}{\hat{e}(X_i)} + \frac{(1 - D_i) \cdot P(D = 0)}{1 - \hat{e}(X_i)},$$

trim extreme weights (1st/99th percentiles), and then estimate the outcome model

$$Y_i = \alpha + \tau D_i + X_i^\top \gamma + \varepsilon_i$$

by weighted least squares using w_i. Standard errors are obtained via nonparametric bootstrap (1,000 replications). This specification is doubly robust: τ is consistent if either the treatment or outcome model is correctly specified. Balance diagnostics and common support are reported in Appendix A.5.

3. Results

3.1. Disadvantaged communities face systematically greater distances to AFCs

DACs are, on average, located significantly farther from AFCs than non-DAC tracts. On average, DACs are located 6.93 miles from the nearest AFC, compared to 4.53 miles for non-DACs; this is a difference of 2.4 miles, or about 53% farther (Table 1). This difference is not driven by outliers but is consistent across the full distribution of tracts (Appendix, Fig. A1).

Table 1: Welch Two Sample t-test comparing mean distance to AFCs between DAC and non-DAC tracts.

Non-DAC	**DAC**	**t**	**df**	**p-value**	**95% CI**
4.53	6.93	-18.3	15,566	¡2.2e-16	[-2.65, -2.14]

3.2. Spatial clustering reveals regional concentration of poor AFC access

We examine the geography of access disparities using Local Moran's I to detect spatial autocorrelation in distance to AFCs. The results, visualized in Figure 1, reveal that poor access is geographically clustered. Areas shaded in red represent high-high clusters: tracts with longer distances to AFCs surrounded by similarly under-served neighbors. Global Moran's I confirms strong spatial clustering in tract-level distances to AFCs ($I = 0.812$, $p < 0.001$), indicating that these patterns reflect systematic spatial dependence rather than random distribution. In particular, clusters of limited AFC access are concentrated in regions such as southern Georgia, Alabama, and eastern Mississippi. Conversely, areas shaded in blue represent spatial outliers: tracts with notably shorter or longer distances to AFCs than their surrounding neighbors. For example, in parts of western North Carolina and central Georgia, some tracts with shorter distances to AFCs are surrounded by neighbors with much longer distances, indicating sharp local contrasts in infrastructure access.

3.3. Spatial spillovers amplify inequalities beyond tract boundaries

We estimate a SDM to assess how disparities in AFC proximity are shaped by both tract-level characteristics and the attributes of neighboring areas. The model decomposes effects into (1) direct effects, which capture how a tract's own characteristics influence access, and (2) indirect effects, which capture how characteristics of neighboring tracts shape a tract's own access.

Table 2 reports decomposed effects for each predictor. Traffic proximity and volume has a total effect of -0.587; $p < 0.001$ on distance to AFC, driven primarily by indirect effects: areas surrounded by dense traffic, which tend to have higher emissions and mobility demand, have significantly closer access to AFCs. $PM_{2.5}$ exposure shows a mixed spatial pattern: tracts with high pollution levels tend to be located closer to AFCs ($direct = -0.198$; $p < 0.001$), while tracts adjacent to those high-pollution areas tend to be located farther from AFCs ($indirect = 0.308$; $p < 0.001$), resulting in a net positive total effect. This spatial mismatch suggests that while core pollution hotspots are prioritized for AFC siting, adjacent areas with comparable burdens remain under-served.

Similarly, tracts with high housing burden ($total = 0.184$; $p = 0.064$) are also associated with reduced access. Meanwhile, tracts with high diesel particulate matter exposure have significantly better access to AFCs ($total = -0.177$; $p = 0.036$), primarily due to strong direct effects. This likely

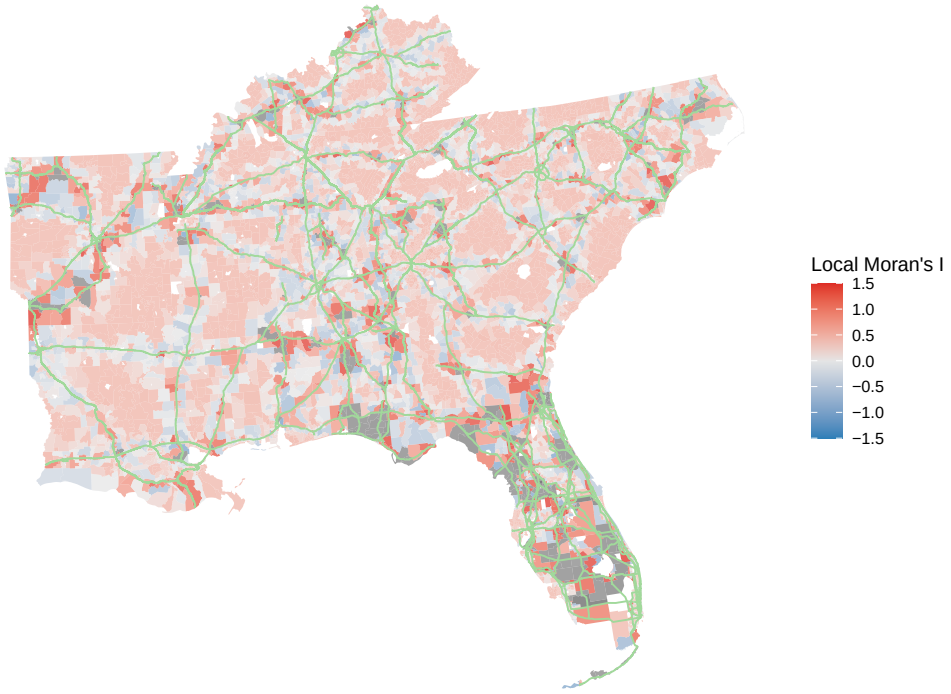


Figure 1: Local Moran's I for tract-level distance to AFCs, excluding tracts with populations below 1,000. Positive values (red) indicate clusters where tracts with greater distance to AFCs are surrounded by similarly underserved neighbors. Negative values (blue) indicate spatial outliers. Gray indicates areas with no significant spatial clustering. Green lines represent AFCs.

reflects the alignment of AFCs with freight corridors and trucking routes that contribute to pollution.

Proximity to highways is strongly associated with better AFC access at the tract-level (0.720; $p < 0.001$), reflecting the highway-based siting rules of NEVI. However, the indirect effect is sharply negative (-0.676; $p < 0.001$), suggesting that tracts located near others that are also close to freeways may still be bypassed. This indicates that NEVI investments are tightly clustered along specific corridors and do not necessarily extend benefits to neighboring areas, even when those areas are also well-positioned in the highway network. In contrast, DAC status does not have a statistically significant direct or indirect effect, suggesting that observed proximity gaps are explained by

Table 2: Decomposed SDM impacts on logged distance to AFCs. Bootstrapped to 1,000 simulations. All variables except DAC status (binary) and freeway distance (logged) are percentiles. The model includes a control for rural–urban classification. Each cell presents the coefficient estimate with 95% confidence interval and p-value. Appendix A.3 reports the full SDM coefficient estimates and robustness checks.

Variable	Direct Effect	Indirect Effect	Total Effect
DAC binary	-0.014 [-0.032, 0.003] p = 0.104	-0.105 [-0.449, 0.240] p = 0.551	-0.119 [-0.476, 0.238] p = 0.514
Poverty rate	0.008 [-0.003, 0.019] p = 0.143	0.119 [-0.096, 0.333] p = 0.279	0.127 [-0.096, 0.350] p = 0.264
Energy burden	0.001 [-0.009, 0.011] p = 0.893	-0.100 [-0.260, 0.059] p = 0.217	-0.100 [-0.265, 0.060] p = 0.235
Agricultural loss rate	0.014 [0.004, 0.023] p = 0.005	-0.051 [-0.166, 0.064] p = 0.384	-0.037 [-0.156, 0.081] p = 0.537
Diesel PM exposure	-0.124 [-0.143, -0.105] p < 0.001	-0.053 [-0.215, -0.108] p = 0.016	-0.177 [-0.343, -0.012] p = 0.036
PM2.5 exposure	-0.198 [-0.286, -0.110] p < 0.001	0.308 [0.193, 0.423] p < 0.001	0.110 [0.036, 0.184] p = 0.003
Traffic proximity & volume	-0.065 [-0.075, -0.055] p < 0.001	-0.522 [-0.692, -0.352] p < 0.001	-0.587 [-0.763, -0.411] p < 0.001
Housing burden	0.002 [-0.009, 0.013] p = 0.743	0.182 [-0.004, 0.368] p = 0.056	0.184 [-0.011, 0.378] p = 0.064
Freeway distance	0.720 [0.707, 0.733] p < 0.001	-0.676 [-0.784, -0.569] p < 0.001	0.044 [-0.064, 0.151] p = 0.424

structural burdens rather than designation alone.

Figure 2 visualizes the spatial distribution of estimated effects from the SDM on tract-level distance to AFCs. Panel A shows the composite direct effect of a tract's own burdens on its AFC access. Panel B shows the indirect (spillover) effects of burdens in neighboring tracts. Panel C combines both into total effects. These maps highlight regions where the joint influence of local and surrounding burdens most strongly shapes AFC access. Panel C reveals that in many areas, indirect effects offset direct effects, emphasizing the importance of spatial interdependencies in producing access inequalities. These findings reveal that AFC deployment under NEVI is spatially uneven, reflecting and reinforcing existing patterns of environmental and socio-economic burdens.

3.4. DAC gaps are mediated by structural burdens and geography

DACs are located significantly farther from AFCs in descriptive comparisons, but the DAC indicator is not statistically significant in the SDM once structural burdens and network geometry are controlled for. To test whether DAC status continues to predict access after accounting for these covariates, we estimated an AIPW model.

Table 3 reports coefficients from an AIPW-weighted OLS of logged distance with covariate adjustment. The DAC coefficient is negative and highly significant ($\hat{\beta} = -0.034$, $p = 0.0012$), corresponding to an estimated $100\big(e^{-0.034}-$

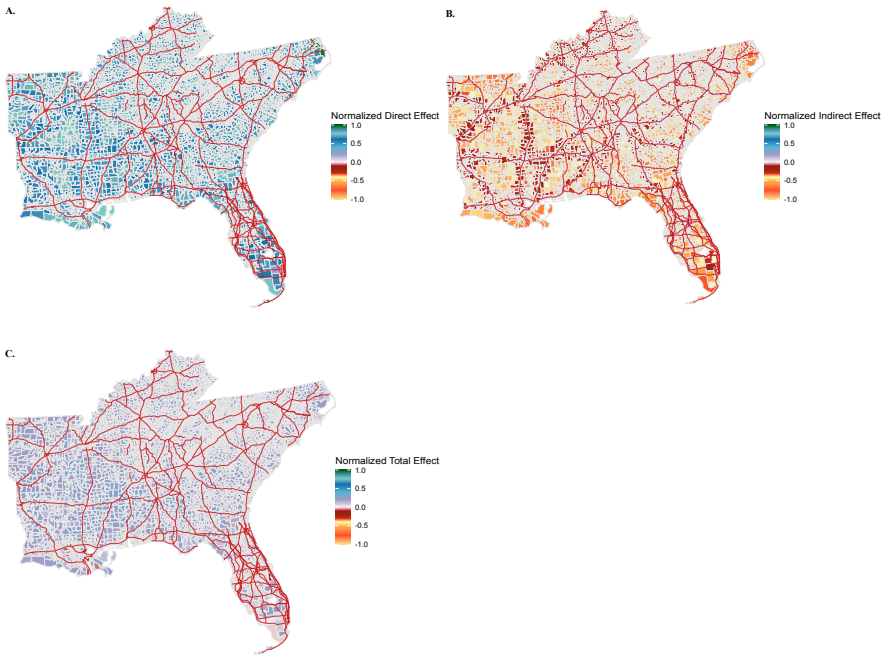


Figure 2: Normalized SDM effects on logged distance to nearest AFCs. Panel A shows direct effects, Panel B shows indirect (spillover) effects, and Panel C shows total effects. Bootstrapped to 1,000 simulations. All predictors are in percentiles except DAC status (binary) and freeway distance (logged).

1) $\approx -3.3\%$ decrease in distance for DAC tracts on average. This pattern indicates that the descriptive DAC gap operates primarily through structural burdens and network proximity rather than the DAC classification.

Table 3: Augmented inverse probability weighted OLS estimates for logged distance to AFC corridors. Weights are stabilized and trimmed at the 1st and 99th percentiles to ensure overlap. The model includes a control for rural–urban classification.

Predictor	Coefficient	Std. Error	p-value
Intercept	0.760	0.0126	< 0.001
DAC Binary	-0.034	0.0104	0.0012
Poverty Rate	0.0257	0.0078	0.0010
Energy Burden	0.0058	0.0074	0.434
Ag. Loss Rate	0.0358	0.0067	< 0.001
Diesel PM	-0.1793	0.0097	< 0.001
PM2.5 Exposure	0.0581	0.0052	< 0.001
Traffic Proximity	-0.1447	0.0082	< 0.001
Housing Burden	0.0061	0.0079	0.437
Freeway Distance (log)	0.4241	0.0065	< 0.001
R^2 (Adj.)			0.573
Residual Std. Error		0.549 (df = 15,244)	

Post-AIPW spatial lag models (Appendix Table A.8) reveal strong and statistically significant spatial dependence in the residuals (Wald and LR tests, $p < 0.001$), underscoring that spatial interdependencies remain important even after covariate adjustment. Taken together, the SDM and AIPW results indicate that the descriptive DAC gap is generated primarily through structural burdens and network proximity; once these are balanced, DAC designation itself is not the independent driver of poorer access. Robustness checks, including alternative DAC definitions and centroid specifications, are reported in Appendix E.

3.5. Equity shortfalls are structural but can be addressed by policy

Equity shortfalls in AFC siting are structural, but they are not immutable. To illustrate, we simulate an equity scenario in which the average distance to AFCs for DACs is reduced by 40%. This was achieved by reallocating AFC distance values from non-DAC tracts to DAC tracts, prioritizing those most disadvantaged, while holding the total number of tracts with AFC access constant. This counterfactual approximates the intent of Justice40 and demonstrates how strategic realignment of AFCs can generate substantial equity gains. As shown in Table 4, this approach closes the proximity gap between DACs and non-DACs and significantly reduces spatial spillovers of disadvantage. The share of DAC tracts within five miles of an

AFC increases from 64.0% to 73.0%, matching non-DACs. Importantly, these improvements extend beyond individual communities: the spatial clustering of exclusion declines markedly. The indirect (spillover) effect shrinks by more than 60%, from -0.105 to -0.038, underscoring that spatial inequality is not fixed, but can be reshaped through targeted policy.

Table 4: Summary of Access Inequality and Spatial Spillover Impacts for DAC Status. Panel A reports direct measures of AFC proximity for DAC and non-DAC tracts under current deployment and the forward-looking equity scenario. Panel B reports spatial Durbin Model impacts for DAC status, decomposing total, direct, and spillover (indirect) effects under current and equity scenarios.

Panel A: Access Distance Summary			
Community Type	**Mean Distance (miles)**	**Median Distance (miles)**	**% Within 5 Miles**
Current Deployment			
Non-DAC	4.53	2.41	71.9%
DAC	6.93	2.57	64.0%
Equity Scenario			
Non-DAC	4.53	2.41	71.9%
DAC	4.16	1.54	73.0%
Panel B: Spatial Spillover Impacts for DAC Status			
Scenario	**Direct Effect**	**Indirect (Spillover)**	**Total Effect**
Current Deployment	-0.014	-0.105	-0.119
	[-0.032, 0.003; p = 0.102]	[-0.453, 0.244; p = 0.556]	[-0.483, 0.232; p = 0.518]
Equity Scenario	-0.335	-0.038	-0.374
	[-0.350, -0.319; p ¡ 0.001]	[-0.137, 0.071; p = 0.556]	[-0.482, -0.042; p = 0.039]

While illustrative, this scenario carries important caveats. It does not incorporate constraints imposed by the existing highway network, such as proximity to highways or NEVI's 50-mile spacing rules. These are core features of NEVI's current siting logic. While this may limit its direct applicability, the simplification allows us to illustrate the effects of prioritizing disadvantaged communities and highlight the redistributive potential of alternative siting strategies. We acknowledge that actual siting decisions are shaped by additional spatial and regulatory constraints, and future work could extend this analysis by incorporating those constraints into a spatial optimization model that more closely reflects real-world deployment dynamics.

4. Discussion & Conclusion

Infrastructure often reflects planning choices, institutional priorities, and bureaucratic routines that tend to reinforce, rather than redress, entrenched inequities in access and investment [1]. In the context of climate policy, equity in the clean energy transition is therefore not merely a challenge of infrastructure expansion, but a spatial governance challenge that determines who benefits from public investment and who is left out. Once in place, infrastructure shapes access and exclusion for decades, locking in spatial patterns of

mobility, investment, and opportunity [10, 26, 27]. Siting decisions are thus not only technical, but political: they define the spatial terms of inclusion in the clean energy economy. Despite NEVI's alignment with the Justice40 initiative, our results show that historically burdened communities are likely to remain structurally farther from AFCs. This is not simply a planning oversight; it reflects how spatial inequality is embedded in the provision of infrastructure.

Our findings show that DACs are systematically located farther from NEVI-proposed AFCs, even after controlling for rural–urban status and existing highway access. These disparities are not fully explained by tract-level demographic or environmental burdens. Instead, they reflect broader spatial patterns shaped by legacy infrastructure, uneven regional connectivity, and planning frameworks that have historically failed to ensure equitable access. In this context, disadvantage is not simply about who a community is, but where it is. The geography of NEVI's proposed deployment places many DACs in locations structurally disconnected from high-priority corridors, extending spatial exclusion into the clean energy transition [28, 11].

Our analysis also reveals that the role of DAC designation is more complex than descriptive comparisons alone suggest. In the SDM, the DAC indicator is not statistically significant once structural burdens and network proximity are controlled for. Similarly, in the AIPW analysis, the DAC coefficient is negative, indicating that after balancing covariates, DACs are not independently farther from AFCs. This apparent reversal highlights that disadvantage operates primarily through the structural and geographic burdens disproportionately borne by DACs rather than through the DAC classification itself. This reinforces our interpretation that access shortfalls are structural rather than incidental to classification.

A key contribution of this study is to reveal how spatial spillovers compound disadvantage across regions. Existing equity frameworks like Justice40 emphasize distributive fairness within communities but ignore the spatial dynamics between communities. Our findings show that poor access to EV infrastructure is not randomly distributed but spatially clustered: disadvantaged communities and their neighboring tracts are jointly underserved. These spillover effects create regional pockets of exclusion, where lack of infrastructure in one area reduces the connectivity and economic opportunity of adjacent areas as well. In this way, spatial inequality compounds structural disadvantage not just within, but across, communities [29, 30, 2]. Addressing these patterns will require moving beyond place-based equity to embrace

spatially relational approaches that confront the geographic reproduction of exclusion.

Greater distance from AFC infrastructure signals reduced access to federally supported mobility systems and exclusion from the material benefits of public investment. This may limit the likelihood of future infrastructure upgrades, improved air quality, and grid enhancements, particularly in communities already burdened by environmental and economic stressors. These effects are amplified by spatial spillovers: when disadvantaged tracts are clustered together, the broader region becomes less likely to attract infrastructure investment. This can occur even when some communities within the cluster are well-positioned for AFC development when viewed in isolation. Because infrastructure begets infrastructure, greater distance becomes a proxy for exclusion from emergent systems of clean mobility and opportunity.

These findings also carry important implications for how equity is operationalized in federal infrastructure governance. While Justice40 articulates ambitious equity goals, its siting rules lack proximity thresholds or spatial distribution criteria. Consequently, NEVI planning defaults to technical metrics, such as traffic volume, interconnectivity, and cost-efficiency that privilege high-throughput corridors and bypass marginalized areas. This procedural vagueness renders equity largely symbolic unless it is tied to spatially grounded mandates. Failure to embed spatial criteria into planning allows structurally exclusionary systems to persist under the guise of technocratic neutrality [31].

The absence of clear siting guidelines in NEVI reflects a broader tension in clean energy transitions: different ideas about what fairness means in infrastructure planning often conflict. Should chargers be distributed equally across all areas? Should they be prioritized for the communities with the greatest need? Or concentrated in places that maximize efficiency and usage? These trade-offs are rarely acknowledged, yet they shape who gains access to clean energy infrastructure. NEVI's current siting approach appears to favor proportionality and network efficiency, reinforcing technocratic principles that emphasize throughput over equity. Reducing access disparities for historically under-served communities requires a corrective distributive approach—one that explicitly prioritizes structurally disadvantaged areas. Without making these normative commitments transparent, equity frameworks risk becoming rhetorical instruments rather than enforceable design principles [2].

Even with its limitations, our simulation underscores a critical insight:

infrastructure disadvantage is not a spatial inevitability; it is a policy outcome. By demonstrating how a modest reallocation can reduce both direct and spillover disparities, the scenario highlights the transformative potential of spatially explicit mandates, such as regional siting thresholds or minimum DAC coverage targets. Without such mandates, the clean energy transition risks replicating the geography of the fossil fuel economy [32, 2]. But realizing this promise demands more than analytic tools; it requires institutional reform. Embedding spatial justice into infrastructure governance is not only normatively essential but practically necessary. It ensures that transitions are not only technologically sound and economically efficient, but socially legitimate and democratically accountable.

Acknowledgement

This research was supported by the University of Georgia's E-Mobility Seed Grant program and by the National Science Foundation (grants 2343136, 2420985, and 2242507). The authors are grateful to participants at the 2024 Midwest Political Science Association Conference and to colleagues at the River Basin Center for their helpful feedback on earlier versions of this paper. The authors declare no financial or other conflicts of interest.

Appendix A. Supplementary Data, Methods, and Results

Table A.5: Variables Used in Analysis and Corresponding Justice40 Burden Categories

Variable	**Justice40 Burden Category**
DAC Binary	Not a burden category; binary designation for DAC
Poverty Burden (Percentile)	Health & Housing
Energy Burden (Percentile)	Energy
Housing Burden (Percentile)	Housing
Expected Agriculture Loss Rate (Percentile)	Climate Change
Diesel Particulate Matter Exposure (Percentile)	Health
PM2.5 Exposure (Percentile)	Health
Traffic Proximity and Volume (Percentile)	Transportation
Freeway Distance (logged)	Not in Justice40; included as geographic control

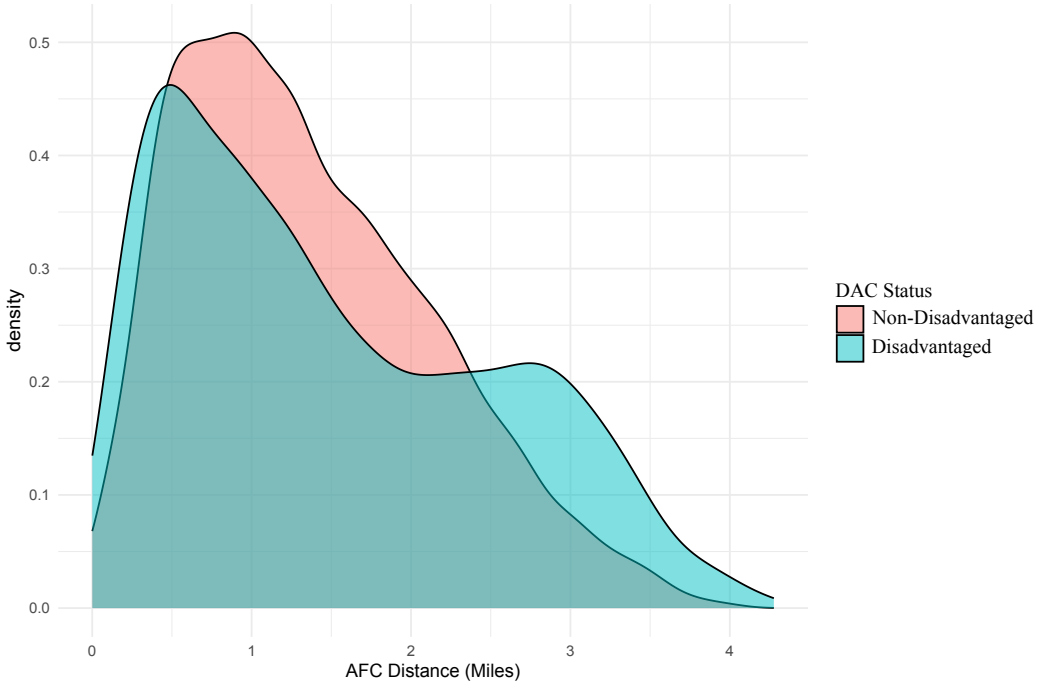


Figure A.3: Distribution of tract-level distance to AFCs by DAC status. Density plots show that DACs are systematically farther from AFCs than non-DAC tracts. The right-shifted distribution for DACs indicates that the difference in proximity is consistent across the entire distribution, not driven by outliers.

Appendix A.1. Spatial Dependence Diagnostics

Table A.6: Global Moran's I Tests for Spatial Autocorrelation. Moran's I statistics indicate strong and statistically significant positive spatial autocorrelation in both the raw log distance to AFC corridors and the residuals from a covariate-adjusted OLS model. The high Moran's I values and low p-values confirm spatial clustering and support the need for spatial econometric modeling.

Test Variable	Moran's I	Expectation	p-value
Log Distance to AFC Corridors (raw variable)	0.8116	-0.00006	< 0.001
OLS Residuals (model with covariates)	0.8734	-0.00006	< 0.001

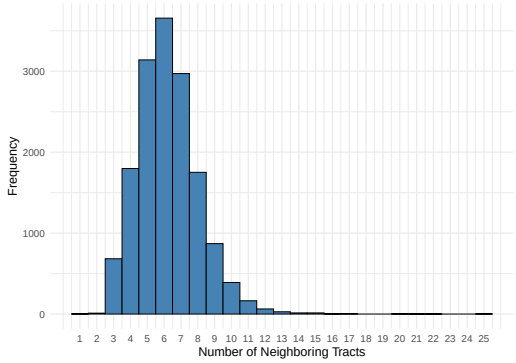


Figure A.4: Distribution of the number of neighboring tracts under a first-order Queen contiguity criterion. Neighborhood sizes range from 1 to 25 tracts, with a median of 6. This structure captures both edge and vertex adjacency and forms the basis for the spatial weights matrix used in the Spatial Durbin Model.

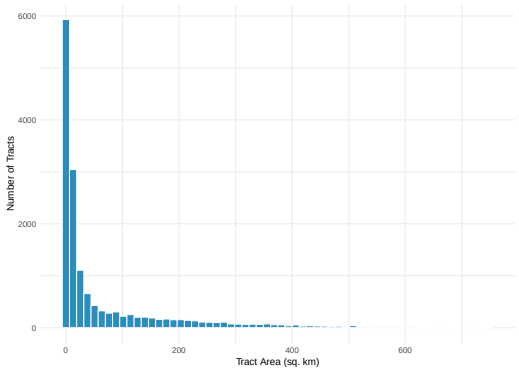


Figure A.5: Distribution of census tract area (in square kilometers) across the ten southeastern U.S. states included in the study. Tract sizes range from less than 1 km^2 to over 600 km^2, with a right-skewed distribution and a median of approximately 123 km^2. This spatial heterogeneity underscores the use of geometric centroids and spatial econometric methods in the analysis.

Table A.7: Lagrange Multiplier (LM) Tests for Spatial Dependence in OLS Residuals. These tests assess whether residuals from the non-spatial OLS model exhibit spatial autocorrelation. All tests reject the null hypothesis of no spatial dependence at the 0.001 significance level. The robust LM tests confirm the presence of both spatial error and spatial lag dependence, justifying the use of a SDM.

Test Description	Test Statistic	p-value
LM Test for Spatial Error Dependence (RSerr)	23,859	< 0.001
LM Test for Spatial Lag Dependence (RSlag)	21,758	< 0.001
Robust LM Error Test (adjRSerr)	2,183.3	< 0.001
Robust LM Lag Test (adjRSlag)	82.25	< 0.001
SARMA Test (joint error + lag dependence)	23,941	< 0.001

Appendix B. Multicollinearity Checks

Table B.8: Variance Inflation Factors (VIF) for OLS Model Predictors. All VIF values fall well below the common threshold of 10, indicating no evidence of problematic multicollinearity among the explanatory variables. This supports the stability and interpretability of coefficient estimates in the spatial regression models.

Predictor Variable	VIF
Diesel PM Exposure	3.98
Poverty Rate	3.26
Traffic Proximity	2.79
Housing Burden	2.83
Energy Burden	2.76
Disadvantaged Status	2.08
Agricultural Loss Rate	1.96
Freeway Distance (log)	1.89
$PM_{2.5}$ Exposure	1.14

Appendix C. Model Selection Comparison

Table C.9: Comparison of Spatial Regression Models: Spatial Lag (SLM), Spatial Error (SEM), and Spatial Durbin Model (SDM). The dependent variable is the logged distance to the nearest AFC corridor. The SDM outperforms both SLM and SEM across key fit metrics, including log likelihood, residual variance, and AIC. High and statistically significant spatial coefficients in all models confirm strong spatial dependence. The SDM also resolves nearly all residual autocorrelation (Moran's I LM test = 15.81; $p < 0.001$), supporting its use as the preferred specification.

Model Statistic	SLM	SEM	SDM
Number of observations	15,566	15,566	15,566
Log likelihood	-7,124.666	-2,353.599	-2,243.105
Residual variance (σ^2)	0.1187	0.0606	0.0606
Spatial coefficient (ρ or λ)	0.8899	0.9527	0.9407
Asymptotic SE of spatial coefficient	0.0036	0.0025	0.0028
z-value (spatial coefficient)	247.08	384.51	338.91
Wald test for spatial dependence	61,048; $p < 0.001$	147,840; $p < 0.001$	114,860; $p < 0.001$
Likelihood ratio (LR) test	17,809; $p < 0.001$	22,853; $p < 0.001$	22,485; $p < 0.001$
LM test for residual autocorrelation	266.73; $p < 0.001$	—	15.81; $p = 0.00007$
Akaike Information Criterion (AIC)	14,271	4,731.2	4,528.2
Spatial weights matrix	Row-standardized Queen	Row-standardized Queen	Row-standardized Queen

Appendix D. SDM Results and Robustness Checks

Table D.10: Spatial Durbin Model (SDM) Coefficient Estimates. This table reports the full coefficient estimates from the SDM used to model logged distance to AFC corridors. The model includes a spatial lag of the dependent variable ($\rho = 0.940$) and spatial lags of all covariates. A row-standardized Queen contiguity matrix defines spatial relationships. Standard errors are asymptotic.

Variable	**Estimate**	**Std. Error**	**p-value**
Intercept	0.0803	0.0076	< 0.001
Disadvantaged Status (DAC)	-0.0109	0.0061	0.073
Poverty Rate	0.0038	0.0038	0.322
Energy Burden	0.0026	0.0046	0.568
Ag. Loss Rate	0.0119	0.0045	0.008
Diesel PM	-0.1670	0.0108	< 0.001
$PM_{2.5}$ Exposure	-0.1692	0.0475	< 0.001
Traffic Proximity	-0.0486	0.0042	< 0.001
Housing Burden	-0.0029	0.0036	0.429
Freeway Distance (log)	0.7316	0.0073	< 0.001
Rural Indicator	0.0079	0.0110	0.469
Spatially Lagged Covariates			
Lagged DAC Status	-0.0040	0.0114	0.726
Lagged Poverty Rate	0.0022	0.0069	0.748
Lagged Energy Burden	-0.0090	0.0065	0.166
Lagged Ag. Loss Rate	-0.0135	0.0058	0.020
Lagged Diesel PM	0.1619	0.0120	< 0.001
Lagged $PM_{2.5}$ Exposure	0.1755	0.0478	< 0.001
Lagged Traffic Proximity	0.0150	0.0066	0.023
Lagged Housing Burden	0.0166	0.0064	0.009
Lagged Freeway Distance (log)	-0.7293	0.0084	< 0.001
Lagged Rural Indicator	0.0252	0.0136	0.063
Spatial Lag of Dependent Variable (ρ)	0.9396	0.0028	< 0.001
Residual Variance (σ^2)			0.0603
Log Likelihood			-2198.003
AIC			4442.0
Sample Size			15,549 tracts

Table D.11: Residual Diagnostic Tests for Model Assumptions. The Breusch–Pagan test, run on the OLS baseline model, indicates significant heteroskedasticity, supporting the use of bootstrapped standard errors in the SDM. The Jarque–Bera test shows that SDM residuals deviate from normality, a common feature in large spatial datasets. The low Moran's I value suggests minimal residual spatial autocorrelation. Sample size is 15,566 census tracts.

Test	Statistic	df	p-value
Global Moran's I (SDM residuals)	0.0131	–	0.0023
Breusch–Pagan (OLS residuals)	1942.0	9	< 0.001
Jarque–Bera (SDM residuals)	71,224.0	2	< 0.001

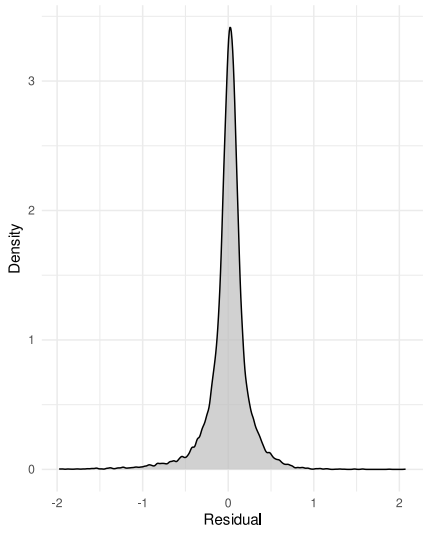


Figure D.6: Density plot of residuals from the SDM. The distribution is approximately centered around zero, indicating no systematic bias. The shape is uni-modal and reasonably symmetric, suggesting acceptable model specification with respect to residual distribution.

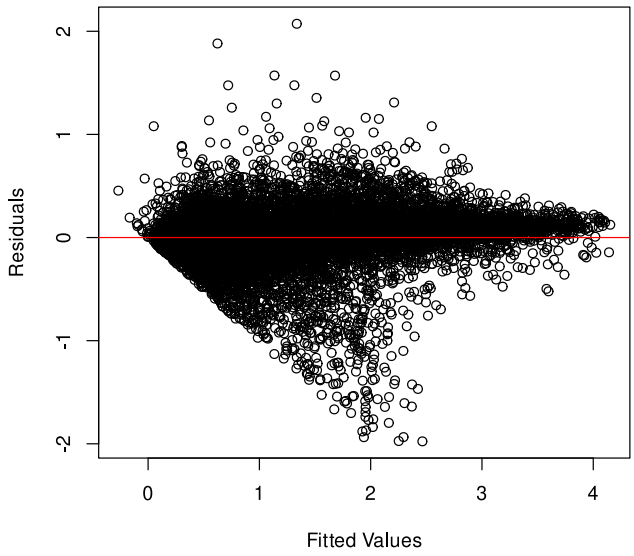


Figure D.7: Residuals versus fitted values from the SDM. While residuals are generally centered around zero, the funnel-like pattern suggests mild heteroskedasticity, particularly at lower fitted values. However, the overall structure does not indicate model misspecification severe enough to invalidate the results, especially given the reduced spatial autocorrelation in residuals.

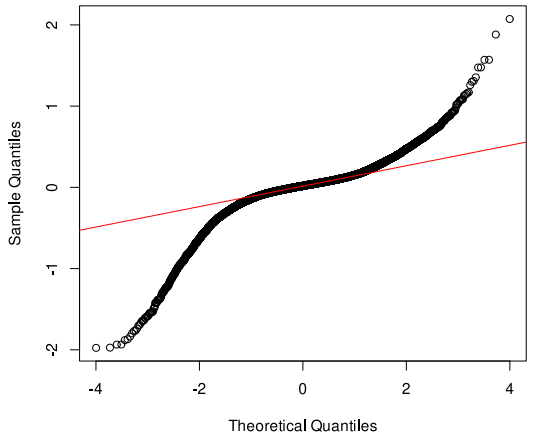


Figure D.8: Normal Q-Q plot of residuals from the SDM. The residuals generally follow a normal distribution, though there is modest deviation in the tails. This pattern is common in large spatial datasets and does not suggest substantial violation of normality assumptions that would undermine inference.

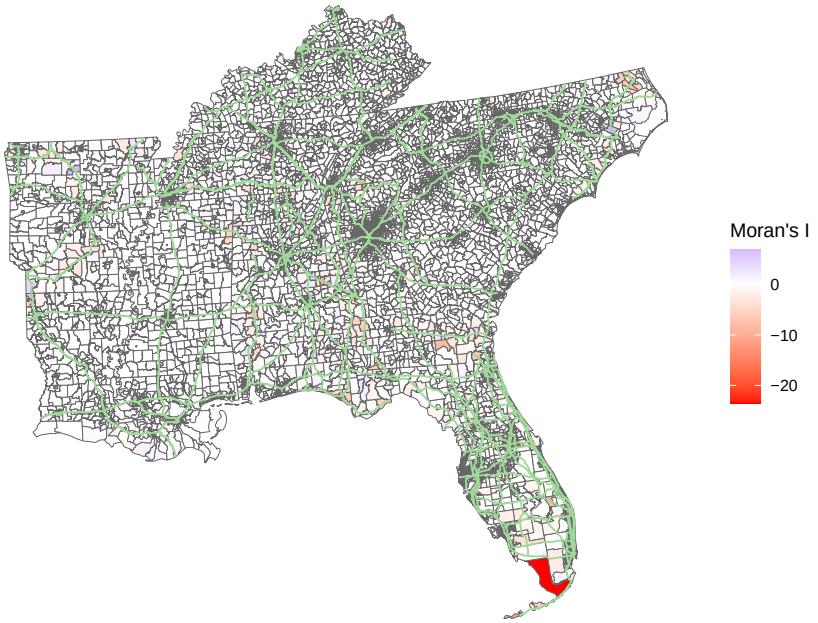


Figure D.9: This map visualizes the spatial distribution of Local Moran's I values for residuals from the SDM. Blue areas indicate positive spatial autocorrelation in residuals (clusters of similar values), while red areas represent negative spatial autocorrelation (spatial outliers). Most tracts show Moran's I values near zero, suggesting weak or negligible residual spatial dependence across much of the study area. This reinforces the finding from the global Moran's I test that residual autocorrelation is minimal (Moran's I = 0.013; p = 0.0023), supporting the adequacy of the SDM specification.

Appendix E. Inverse Probability Weights Analysis

To further test for residual spatial dependence, we estimate two spatial lag models. The first uses residuals from the IPW-weighted OLS regression as a covariate (Column 1, Table E.12), while the second regresses the residuals themselves as the dependent variable in a spatial lag model (Column 2, Table E.12). The first model yields a small and bounded spatial coefficient ($\rho = 0.074$), suggesting that residual dependence is largely addressed by the IPW adjustment. The second model, however, shows a high spatial autocorrelation coefficient ($\rho = 0.946$), indicating that while spatial processes remain embedded in the residual distribution, they are not driving the IPW model's estimates.

Table E.12: Post-IPW Spatial Lag Models to Test for Residual Spatial Dependence.

Model Statistic	Residuals as Covariate	Residuals as Outcome
Spatial Coefficient (ρ)	0.074	0.946
Asymptotic SE of ρ	0.0028	0.0027
Wald Statistic	687.8; $p < 0.001$	126,540; $p < 0.001$
Likelihood Ratio Test	671.8; $p < 0.001$	25,293; $p < 0.001$
Log Likelihood	12,390.42	-8,258.30
Residual Variance (σ^2)	0.0119	0.1304
AIC	-24,773	16,523

Appendix E.1. Inverse Probability Weighting Diagnostics

To assess the validity of our inverse probability weighting (IPW) approach, we report balance diagnostics, effective sample size, and overlap visualization for the trimmed and stabilized model.

Overlap:. Figure E.10 displays the estimated propensity score distributions for DAC and non-DAC tracts after trimming observations outside the 1st and 99th percentiles. The density curves show strong overlap between the groups, indicating that the common support assumption is satisfied.

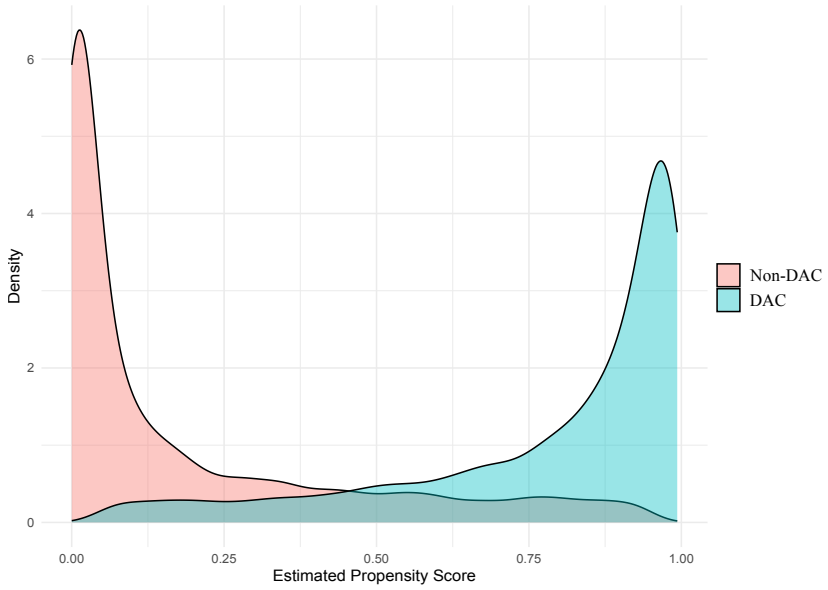


Figure E.10: Propensity score distributions after trimming at the 1st and 99th percentiles. DAC and non-DAC tracts show strong overlap.

Covariate Balance:. Table E.13 presents standardized mean differences (SMDs) for covariates before and after weighting. While balance is improved overall, a few covariates remain moderately imbalanced (e.g., poverty, energy burden, housing burden), with post-weighting SMDs exceeding 0.25.

Table E.13: Covariate balance summary before and after applying inverse probability weights. Reported values are standardized mean differences (SMDs) after weighting.

Covariate	SMD (After Weighting)
Propensity Score	0.737
Poverty Rate	0.778
Energy Burden	0.697
Ag. Loss Rate	0.024
Diesel PM Exposure	−0.074
PM2.5 Exposure	−0.025
Traffic Proximity	0.002
Housing Burden	0.446
Freeway Distance (log)	0.075

Visual Balance Plot.. Figure E.11 provides a visual summary of covariate balance before and after weighting. The dashed vertical line at 0.1 marks the conventional threshold for strong balance; covariates above 0.25 may still exhibit imbalance.

Effective Sample Size.. After trimming and stabilization, the effective sample size (ESS) is estimated at 6,577 observations. This reflects a substantial retention of statistical information and mitigates the influence of extreme weights.

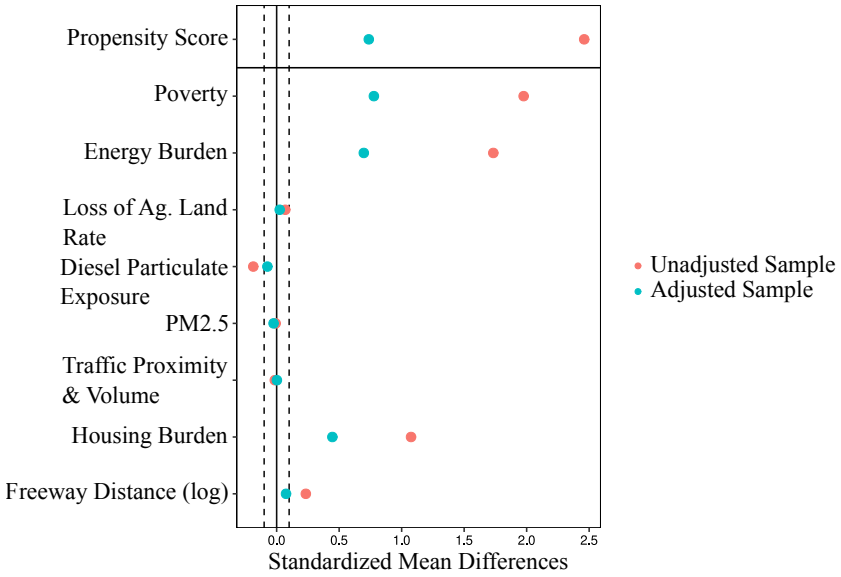


Figure E.11: Love plot showing standardized mean differences before and after weighting. Covariates to the right of the vertical line (SMD ¿ 0.25) are considered moderately imbalanced, even after weighting.

References

[1] B. Pandey, C. Brelsford, K. C. Seto, Infrastructure inequality is a characteristic of urbanization, Proceedings of the National Academy of Sciences 119 (2022) e2119890119.

[2] P. Lehmann, E. Gawel, J.-N. Meier, M. J. Reda, F. Reutter, S. Sommer, Spatial distributive justice has many faces: The case of siting renewable energy infrastructures, Energy Research & Social Science 118 (2024) 103769.

[3] L. M. Aiello, A. Vybornova, S. Juhász, M. Szell, E. Bokányi, Urban highways are barriers to social ties, Proceedings of the National Academy of Sciences 122 (2025) e2408937122.

[4] D. Karas, Highway to inequity: the disparate impact of the interstate highway system on poor and minority communities in american cities, New Visions for Public Affairs 7 (2015) 9–21.

[5] R. Reft, A. P. de Lucas, R. Retzlaff, Justice and the interstates: The Racist truth about urban highways, Island Press, 2023.

[6] N. Anand, A. Gupta, H. Appel, The promise of infrastructure, Duke University Press, 2018.

[7] P. T. Greiner, R. G. McKane, Does racism have inertia? a study of historic redlining's impact on present-day associations between development and air pollution in us cities, Environmental research letters 17 (2022) 104008.

[8] H. M. Lane, R. Morello-Frosch, J. D. Marshall, J. S. Apte, Historical redlining is associated with present-day air pollution disparities in us cities, Environmental science & technology letters 9 (2022) 345–350.

[9] S. Carley, D. M. Konisky, The justice and equity implications of the clean energy transition, Nature Energy 5 (2020) 569–577.

[10] A. Helmrich, M. Chester, T. R. Miller, B. Allenby, Lock-in: origination and significance within infrastructure systems, Environmental Research: Infrastructure and Sustainability 3 (2023) 032001.

[11] C. Robinson, S. Lindley, S. Bouzarovski, The spatially varying components of vulnerability to energy poverty, Annals of the American Association of Geographers 109 (2019) 1188–1207.

[12] S. Conley, D. M. Konisky, M. Mullin, Delivering on environmental justice? us state implementation of the justice40 initiative, Publius: The Journal of Federalism 53 (2023) 349–377.

[13] Q. Yu, T. Que, L. J. Cushing, G. Pierce, K. Shen, M. Kejriwal, Y. Yao, Y. Zhu, Equity and reliability of public electric vehicle charging stations in the united states, Nature Communications 16 (2025) 1–13.

[14] C.-W. Hsu, K. Fingerman, Public electric vehicle charger access disparities across race and income in california, Transport Policy 100 (2021) 59–67.

[15] G. Carlton, S. Sultana, Transport equity considerations in electric vehicle charging research: a scoping review, Transport Reviews 43 (2023) 330–355.

[16] A. M. Varghese, N. Menon, A. Ermagun, Equitable distribution of electric vehicle charging infrastructure: A systematic review, Renewable and Sustainable Energy Reviews 206 (2024) 114825.

[17] Federal Highway Administration, National electric vehicle infrastructure (nevi) program, 2022. URL: https://www.fhwa.dot.gov/environment/nevi/.

[18] Federal Highway Administration, Charging and fueling infrastructure discretionary grant program, 2022. URL: https://www.fhwa.dot.gov/environment/cfi/.

[19] U.S. Department of Transportation, Alternative fuel corridors shapefile, https://hub.arcgis.com/datasets/usdot::alternative-fuel-corridors/explore, 2022. Accessed: May 2024.

[20] U.S. Department of Transportation, Hepgis interstate highway map viewer, https://hepgis-usdot.hub.arcgis.com/pages/852f56ef5f624811bc231aed6da8d7 n.d. Accessed: May 2024.

[21] White House Council on Environmental Quality, Climate & economic justice screening tool: Census tract data, https://screeningtool.geoplatform.gov/en/downloads, 2022. Accessed: May 2024.

[22] J. LeSage, R. K. Pace, Introduction to spatial econometrics, Chapman and Hall/CRC, 2009.

[23] K. Hirano, G. W. Imbens, G. Ridder, Efficient estimation of average treatment effects using the estimated propensity score, Econometrica 71 (2003) 1161–1189.

[24] J. M. Wooldridge, Inverse probability weighted estimation for general missing data problems, Journal of econometrics 141 (2007) 1281–1301.

[25] P. C. Austin, An introduction to propensity score methods for reducing the effects of confounding in observational studies, Multivariate behavioral research 46 (2011) 399–424.

[26] K. C. Seto, S. J. Davis, R. B. Mitchell, E. C. Stokes, G. Unruh, D. Ürge-Vorsatz, Carbon lock-in: types, causes, and policy implications, Annual review of environment and resources 41 (2016) 425–452.

[27] G. C. Unruh, Understanding carbon lock-in, Energy policy 28 (2000) 817–830.

[28] S. Bouzarovski, N. Simcock, Spatializing energy justice, Energy Policy 107 (2017) 640–648.

[29] K. Lucas, Transport and social exclusion: Where are we now?, Transport policy 20 (2012) 105–113.

[30] C. Robinson, S. Bouzarovski, S. Lindley, 'getting the measure of fuel poverty': the geography of fuel poverty indicators in england, Energy research & social science 36 (2018) 79–93.

[31] L. Pulido, Geographies of race and ethnicity ii: Environmental racism, racial capitalism and state-sanctioned violence, Progress in human geography 41 (2017) 524–533.

[32] B. K. Sovacool, R. J. Heffron, D. McCauley, A. Goldthau, Energy decisions reframed as justice and ethical concerns, Nature Energy 1 (2016) 1–6.